ACS OMEGA

Article

Cite This: ACS Omega 2019, 4, 2989−2999

http://pubs.acs.org/journal/acsodf

Water Adsorption on MO_2 (M = Ti, Ru, and Ir) Surfaces. Importance of Octahedral Distortion and Cooperative Effects

Danilo González,[†] Javier Heras-Domingo,[†] Stefano Pantaleone,[†] Albert Rimola, Luis Rodríguez-Santiago, Xavier Solans-Monfort,* and Mariona Sodupe*

Departament de Química, Universitat Autònoma de Barcelona, 08193 Bellaterra, Barcelona, Spain

Supporting Information

ABSTRACT: Understanding metal oxide MO_2 (M = Ti, Ru, and Ir)−water interfaces is essential to assess the catalytic behavior of these materials. The present study analyzes the H_2O−MO_2 interactions at the most abundant (110) and (011) surfaces, at two different water coverages: isolated water molecules and full monolayer, by means of Perdew−Burke−Ernzerhof-D2 static calculations and ab initio molecular dynamics (AIMD) simulations. Results indicate that adsorption preferably occurs in its molecular form on (110)-TiO_2 and in its dissociative form on (110)-RuO_2 and (110)-IrO_2. The opposite trend is observed at the (011) facet. This different behavior is related to the kind of octahedral distortion observed in the bulk of these materials (tetragonal elongation for TiO_2 and tetragonal compression for RuO_2 and IrO_2) and to the different nature of the vacant sites created, axial on (110) and equatorial on (011). For the monolayer, additional effects such as cooperative H-bond interactions and cooperative adsorption come into play in determining the degree of deprotonation. For TiO_2, AIMD indicates that the water monolayer is fully undissociated at both (110) and (011) surfaces, whereas for RuO_2, water monolayer exhibits a 50% dissociation, the formation of $H_3O_2^-$ motifs being essential. Finally, on (110)-IrO_2, the main monolayer configuration is the fully dissociated one, whereas on (011)-IrO_2, it exhibits a degree of dissociation that ranges between 50 and 75%. Overall, the present study shows that the degree of water dissociation results from a delicate balance between the H_2O−MO_2 intrinsic interaction and cooperative hydrogen bonding and adsorption effects.

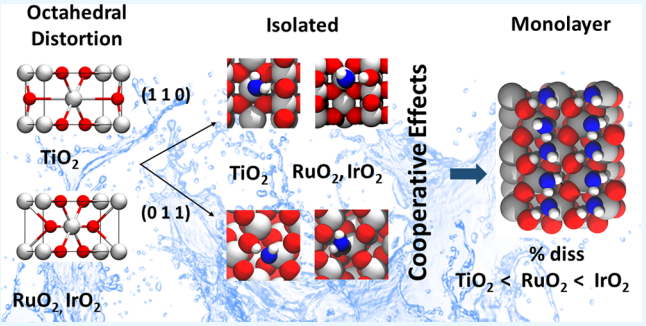

INTRODUCTION

Rutile-like TiO_2, RuO_2, and IrO_2 are isostructural metal oxides with a large number of applications. As an example, they have all been studied for energy conversion and storage from water oxidation either photo- or electrocatalytically.[1−6] Many of these applications imply the existence of a material−water interface, whose understanding is crucial for the rationalization of the global catalytic process. Therefore, the knowledge of the intrinsic water−MO_2 interaction as well as how this interaction varies when increasing the water coverage is of high importance. In this context, several works dealing with H_2O−TiO_2,[7−17] H_2O−RuO_2,[12,13,18−23] and H_2O−IrO_2[13,24,25] interfaces have been reported in the literature. The obtained results allowed determining the different behaviors as a function of the material and the exposed surface. However, some controversy still exists on the amount of water that dissociates after adsorption on the different surfaces and materials.[7]

Among the three materials, titanium oxide is the most intensively explored one. The most stable (110) surface has centered most of the available investigations, which mainly focused on understanding whether water adsorption on this surface dissociates generating H^+/OH^- species.[7,9] The O-defective surfaces have been observed to favor water dissociation, and thus, surface preparation appears to be extremely delicate to determine the intrinsic water−surface interface.[14−16,26] Moreover, results are also sensitive to the experimental conditions and techniques used for the analysis.[9] In this context, several contributions based on high-resolution electron energy loss spectroscopy, temperature-programmed desorption, infrared reflection absorption spectroscopy, and scanning tunneling microscopy (STM) data are in agreement with water adsorbed molecularly on (110),[27−31] particularly at low water coverages. Other experiments performed at higher coverages with X-ray photoelectron spectroscopy (XPS) and photoelectron diffraction techniques suggest that water partially dissociates.[32,33] The reader is referred to the excellent review of *U.* Diebold for a detailed survey of water adsorption on TiO_2 surfaces, the performance of different techniques, and surface preparation.[34] On the other side, density functional theory (DFT) calculations show that the energy difference between the molecular and dissociative adsorption forms is very small and sensitive to the surface model and level of theory used, particularly, the thickness of the slab model, which

Received: November 30, 2018
Accepted: January 25, 2019
Published: February 11, 2019

DOI: 10.1021/acsomega.8b03350
ACS Omega 2019, 4, 2989−2999

exhibits an even−odd behavior, the DFT functional, or the inclusion of the *U* Hubbard correction.[9,10,13,28,35−40] This turns several contributions in favor of one or the other situation. The influence of water coverage on the degree of water dissociation on the (110)-TiO_2 surface has been less addressed and most of the calculations including a water monolayer or more suggest that water adsorbs mainly in its molecular form.[41,42]

Although the interaction between water and the (011) surface of titania has been much less studied, water adsorption at this surface is also relevant because of its large contribution to the Wulff construction. STM, X-ray diffraction measurements, and DFT calculations have shown that the (011) surface suffers an important reconstruction when prepared in ultrahigh vacuum conditions.[11,43−45] This reconstruction is, however, reversed when exposing the distorted (011) surface to liquid water and the original facet is recovered.[11,45] From a computational point of view, calculations suggest that water adsorption at low coverages occurs through the dissociative mode, although increasing the water coverage to the full monolayer seems to decrease the preference for the dissociative form.[11,45−47]

Ruthenium oxide has also been largely studied and again most studies focus on the (110) surface.[12,13,18−23,48] For this (110) surface, it is accepted that at very low coverages, single water adsorbs on unsaturated Ru centers, establishing an equilibrium between molecular and dissociated water molecules.[18−20] Moreover, STM and DFT calculations also indicate that increasing the water coverage allows the formation of water dimers that are adsorbed in contiguous unsaturated Ru centers.[18,19,22] These dimers enclose one molecular and one dissociative water, leading to the formation of $H_3O_2^-$ motifs or hydrogen-bonded $(H_3O_2^-)_n$ chains at higher water coverages. The other (011), (100), and (001) surfaces have only been studied in detail very recently.[21,22] XPS, in situ surface diffraction, and DFT calculations suggest a mixed molecular/dissociative arrangement at high coverages, the ratio between the two forms varying depending on the surface. The two most stable surfaces [(110) and (011)] are more prone to dissociate the adsorbed water, whereas the (001) and (100) surfaces mostly present the molecular form. In our previous paper,[22] observed trends were rationalized by the combination of three factors: (i) the intrinsic acid−base properties of each surface; (ii) the presence of strong cooperative effects; and (iii) an increase of the surface oxygen bridge (O_{br}) basicity by the adsorption of water.

Finally, H_2O−IrO_2 interaction has been much less studied.[13,24,25] To our knowledge, only the adsorption of water on the most stable (110) facet has been addressed by means of DFT calculations. Results suggest that the interaction energy between H_2O and IrO_2 is significantly stronger than in the other two materials and that the adsorbed molecules tend to dissociate.

With the aim of analyzing how the nature of the metal oxide influences the water adsorption and, in particular, the degree of dissociation, we studied the rutile-like H_2O−MO_2 interaction (M = Ti, Ru, or Ir) at the (110) and (011) surfaces, the ones that contribute the most in the Wulff construction of the three materials, considering two different water coverages: isolated water molecules and full monolayer. Moreover, thermal effects and proton mobility on the surface are analyzed by performing ab initio molecular dynamics (AIMD) of the full monolayer coverage. Results show that there are three key factors for determining the degree of dissociative water over the surface: (i) the H_2O−MO_2 intrinsic interaction, (ii) the different octahedral distortion of TiO_2 with respect to RuO_2 and IrO_2, and (iii) the presence of hydrogen bonding and adsorption cooperative effects.

RESULTS AND DISCUSSION

As mentioned above, the main goal of this paper is to compare the properties of MO_2 (M = Ti, Ru, and Ir) upon interacting with water. For that, we first addressed the structural and electronic properties of the bulk and main crystallographic surfaces. Second, we considered the adsorption of one single water molecule at each of the two selected surfaces, with the ultimate goal of comparing the intrinsic water interaction among the three metal oxides. Third, we studied the water monolayer adsorption and evaluated the degree of deprotonation in each case. For that, we carried out, in addition to static calculations, AIMD simulations to address the influence of thermal effects.

MO_2 Bulk and Surfaces. All three considered metal oxides MO_2 (M = Ti, Ru, and Ir) crystallize in a rutile structure, tetragonal with space group $P4_2/mnm$ (see Figure 1a).[49]

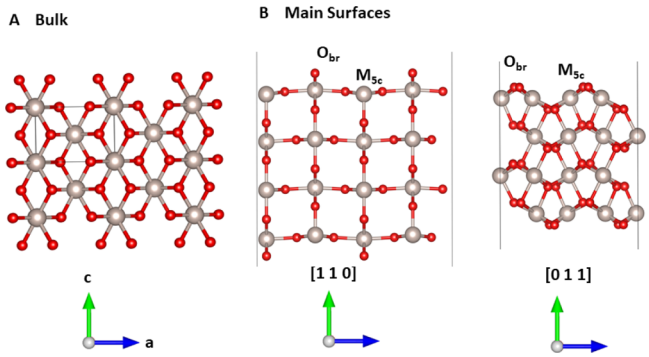

Figure 1. (A) Bulk structure and (B) main surfaces considered in the present work.

Titanium dioxide exhibits two other (thermodynamically metastable) crystalline phases in nature: anatase (tetragonal, $I4_1/amd$) and brookite (rhombohedral, *Pbca*). However, for comparison, the present work will only consider the water adsorption on the rutile polymorph of TiO_2. In the bulk structure, metal cations, M^{4+}, show a distorted octahedral coordination and O^{2-} atoms display a trigonal planar environment. Main distances, cell parameters, and computed net charges of the metal and oxygen atoms for the three metal oxides are given in Table 1.

Concerning the bulk, it can be observed that both M−O distances and cell parameters are in very good agreement with the experimentally determined values,[49] deviations being less than 1.5%. The M−O distances range between 1.95 and 2.01 Å, and the largest ones correspond to IrO_2, as expected. As found experimentally, Ti^{4+} exhibits a distorted octahedral environment with four shorter Ti−O distances in the equatorial plane and two longer Ti−O axial distances (tetragonal elongation), whereas the opposite situation with four longer equatorial M−O distances and two shorter axial ones (tetragonal compression) is observed for RuO_2 and IrO_2. These differences may be related to the electronic configuration of the metal in each metal oxide. That is, the electronic configuration of Ti is $4s^23d^2$, that of Ru is $5s^24d^6$, and that of Ir $6s^15d^8$. Although the metal ion can be formally considered as

DOI: 10.1021/acsomega.8b03350
ACS Omega 2019, 4, 2989−2999

Table 1. MO_2 (M = Ti, Ru, and Ir) Bulk Computed Distances (in Å), Cell Parameters, and Net Atomic Charges (a.u)[a]

	$d(M-O)_{eq}$	$d(M-O)_{ax}$	$d(M-M)$	$a = b$	c	$q(M)$	$q(O)$
TiO_2	1.945	1.990	2.977, 3.579	4.603	2.977	2.240	−1.118
	1.945	*1.986*		*4.594*	*2.959*		
RuO_2	1.997	1.945	3.149, 3.542	4.487	3.149	1.600	−0.750
	1.984	*1.942*		*4.492*	*3.107*		
IrO_2	2.013	1.980	3.193, 3.584	4.497	3.193	1.659	−0.829
	1.998	*1.958*		*4.505*	*3.159*		

[a]Experimental values[49] in italics.

Table 2. Surface Energies (γ in eV Å^{-2}), % of the Surface's Contribution to the Wulff Shape, Main Surface Distances (in Å), and Net Atomic Charges (in a.u)

$(h\ k\ l)$	γ	% Wulff	$d(M-O_{br})$	$d(M_{5/4c}-O)_{eq}$	$d(M_{5/4c}-O)_{ax}$	$d(M-M)$	$q(M_{5/4c})$	$q(O_{br})$
				TiO_2				
(1 1 0)	0.042	70.4	1.833	1.965	1.792	2.977	2.16	−0.99
(0 1 1)	0.074	29.3	1.810, 1.888	1.810, 2.164	1.886, 2.036	3.293	2.19	−1.04
(1 0 0)	0.060	0.0	1.854	1.854, 2.073	1.833	2.977	2.17	−1.02
(0 0 1)	0.085	0.3	1.845, 1.901	1.901	1.787	4.603	2.13	−1.08
				RuO_2				
(1 1 0)	0.098	40.0	1.918	1.982	1.881	3.131	+1.6	−0.75
(0 1 1)	0.105	51.8	1.873	1.873, 2.086	1.955	3.670	+1.64	−0.78
(1 0 0)	0.119	8.2	1.925	1.925, 2.028	1.900	3.130	+1.65	−0.75
(0 0 1)	0.134	0.0	1.842, 1.932	1.918	1.842	4.480	+1.54	−0.81
				IrO_2				
(1 1 0)	0.150	40.3	1.982	2.012	1.943	3.187	1.47	−0.70
(0 1 1)	0.158	53.1	1.897, 1.926	2.000, 2.077	2.000	3.708	1.54	−0.74
(1 0 0)	0.185	6.6	1.960	1.960, 2.034	1.985	3.187	1.50	−0.71
(0 0 1)	0.206	0.0	1.905, 1.992	1.955	1.905	4.541	1.45	−0.77

M^{4+} and thus there are no d electrons in Ti^{4+}, Ru^{4+} has four d electrons, and Ir^{4+} has five d electrons, there is a certain covalent character, and in an octahedral ligand field, this can lead to different geometrical distortions for early and late transition metals. Furthermore, for both RuO_2 and IrO_2, spin-polarized Perdew−Burke−Ernzerhof (PBE)-D calculations indicate that magnetization of each metal ion is equal to zero, as found previously at this level of theory.[50−52] Finally, and as expected, computed charges indicate that TiO_2 is significantly more ionic than RuO_2 and IrO_2.

Slab models for different crystallographic orientations [(110), (011), (100), and (001)] were built cutting out the slab from the optimized bulk structure. Surface energies, main M−O distances of the outermost layer, and net atomic charges are given in Table 2. Values corresponding to the internal layers are very similar to the bulk values and thus have not been included and will not be discussed further.

In all cases, bulk cutting to generate slab models leads to two-coordinated bridging oxygen O_{br} at the surface, as well as five-coordinated M_{5c} sites for (110), (011), and (100) and four-coordinated M_{4c} for (001). The vacant site of M_{5c} in the (110) and (100) surfaces is axial, whereas the vacant site of M_{5c} in the (011) surface is equatorial. For the M_{4c} sites in the (001) facet, both vacant sites are equatorial. Surface M−O distances corresponding to unsaturated M sites vary depending on the coordination environment, the shortest values being found for the axial M_{4c}−O bonds of the (001) surface. M−M distances largely vary depending on the crystal facet and range between 3 and 4.5 Å. For all materials, the shorter values are found in the (110) and (100) surfaces, whereas the larger ones are found for (001).

Computed values for the surface energies are similar to those previously reported in the literature and follow the same trend.[53] That is, the smallest surface energy corresponds to the (110) facet, whereas the largest one corresponds to the (001) one with M_{4c} unsaturated metal centers. The remaining two surfaces show intermediate values, and their relative order depends on the material. For TiO_2, (100) is more stable than the (011) one, whereas for RuO_2 and IrO_2, the relative stability is reversed. Despite that, the contribution of the (100) surface to the TiO_2 Wulff shape is zero, whereas (011) accounts for 29.3% because of symmetry equivalences. Overall, it can be observed in Figure 2 and Table 2 that the (110) and (011) facets contribute by more than an 80% of the total surface, and thus, these two surfaces are the ones considered to analyze the water adsorption.

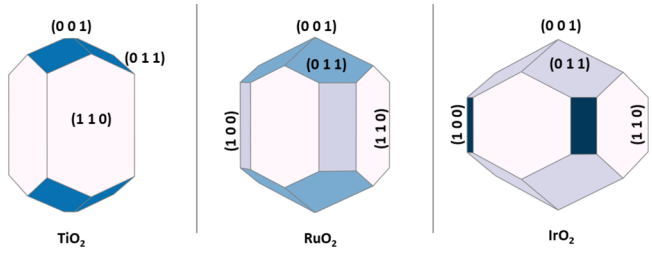

Figure 2. Wulff constructed equilibrium shapes for rutile-like MO_2 (M = Ti, Ru, and Ir).

Adsorption of Isolated Water Molecules. As mentioned above, the aim of the present work is to get insights into the different behavior of MO_2 (M = Ti, Ru, and Ir) upon interacting with water. For that, we first studied the adsorption

DOI: 10.1021/acsomega.8b03350
ACS Omega 2019, 4, 2989−2999

of a single water molecule onto the two surfaces that contribute the most to the Wulff shape (Figure 2): the (110) and (011) surfaces (Figure 1B). This corresponds to a water coverage of 1/4 for (110) and of 1/8 for (011). The preferred adsorption configuration at the (110) and (011) surfaces of MO_2 is that in which the water molecule binds through its O atom with the undercoordinated M_{5c} sites.[10] This interaction increases the water acidity, leading to the formation of a hydrogen bond between one H atom of the water molecule and the nearest undercoordinated O_{br}. This interaction can also lead to a dissociative OH^-/H^+ adsorbed form, with water deprotonated and the O_{br} protonated. Thus, both adsorbed forms, molecular (*mol*) and dissociative (*diss*), have been considered in each of the two surfaces (see Figure 3). Adsorption energies, relative stabilities between the two forms, and main structural parameters are given in Table 3.

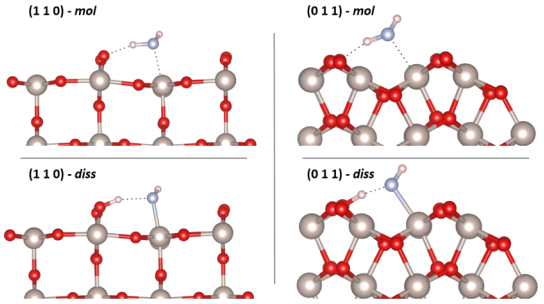

Figure 3. Molecular and dissociative adsorbed forms in the (110)-MO_2 and (011)-MO_2 surfaces.

Regarding the (110) surface, both the molecular and dissociative minima were localized for TiO_2 and RuO_2, whereas only the adsorbed dissociative form was located in the case of IrO_2 in agreement with previous calculations.[9,13,18] Indeed, all attempts to optimize the molecular adsorbed minimum collapsed to the dissociative adsorbed species. Furthermore, results show that while the molecular form is more stable for TiO_2, the dissociative form is more stable for RuO_2 and the only minimum for IrO_2. This is related to the strength of the M−H_2O interaction, which follows the trend: H_2O−TiO_2 < H_2O−RuO_2 < H_2O−IrO_2; that is, the adsorption energy increases (in absolute value) from TiO_2 to IrO_2. As a consequence, the acidity of the water molecule upon interacting with the undercoordinated M_{5c} sites of the surface exhibits a larger increase when it is adsorbed on IrO_2 than on RuO_2 or on TiO_2. This is in agreement with the computed charge of the water molecule in H_2O−MO_2 (M = Ti, Ru, and Ir), which increases from M = Ti to Ir. Thus, despite the higher basicity of O_{br} in TiO_2, as indicated by the net atomic charge of O_{br} (Table 3) and the density of states (DOS), which shows that p bands of O_{br} in TiO_2 lie at higher energy (see Figure 4), the increase of water acidity upon adsorption is not sufficient to favor the dissociative form.

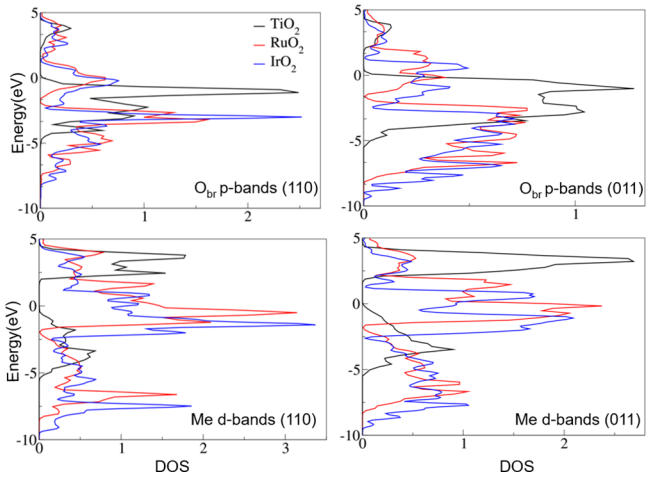

Figure 4. Projected DOS (pDOS) associated with the O_{br} 2p bands and metal d bands.

The computed preference of a single water to be molecularly adsorbed form on (110)-TiO_2 is in agreement with the recent carefully conducted molecular beam/STM experiments by Wang et al.,[9] which determine that molecular adsorption is preferred by 0.035 eV. It should be noted that whether or not water adsorbs in a molecular or a dissociative form on a defect-free TiO_2 (110) surface has been a subject of intense debate.[7] From a computational point of view, different works agree with the fact that the energy difference between *mol* and *diss* is small and sensitive to the computational approximation.[9,10,36,37]

A significantly different behavior is observed for the (011) surface. At this surface, the *diss* form is the most stable adsorbed species on TiO_2, whereas the *mol* form is the

Table 3. Adsorption Energies (ΔE_{ads} in kJ mol^{-1}), Relative Stabilities between the Molecular and Dissociated Forms (ΔE_{rel} in kJ mol^{-1}), Main Distances (in Å), and Net Atomic Charges

		ΔE_{ads}	ΔE_{rel}	O_w−H_w	O_{br}−H_w	M−O_w	$q(H_w)$	$q(O_w)$	$q(O_{br})$	q(M)
					(110)					
TiO_2	*mol*	−86.9	0.0	1.001	1.794	2.251	0.643	−1.22	−1.06	2.23
	diss	−52.2	34.7	1.954	0.994	1.876	0.642	−1.12	−1.22	2.24
RuO_2	*mol*	−131.3	0.0	1.038	1.588	2.172	0.634	−1.17	−0.87	1.67
	diss	−139.6	−8.3	1.754	1.011	1.993	0.660	−1.06	−1.08	1.68
IrO_2	*diss*	−211.5		1.614	1.014	2.018	0.725	−1.13	−1.09	1.68
					(011)					
TiO_2	*mol*	−136.2	0.0	1.044	1.510	2.103	0.654	−1.23	−1.13	2.22
	diss	−140.0	−3.7	1.555	1.028	1.911	0.665	−1.18	−1.24	2.22
RuO_2	*mol*	−115.4	0.0	1.021	1.615	2.177	0.624	−1.17	−0.89	1.73
	diss	−102.8	12.6	1.754	1.011	1.993	0.640	−1.08	−1.04	1.79
IrO_2	*mol*	−152.9	0.0	1.043	1.549	2.108	0.703	−1.24	−0.86	1.65
	diss	−145.9	7.0	1.372	1.110	2.025	0.690	−1.12	−1.01	1.69

DOI: 10.1021/acsomega.8b03350
ACS Omega 2019, 4, 2989−2999

Table 4. Adsorption Energy (ΔE_{ads} in kJ mol^{-1}) per Water Molecule and Main Distances (in Å)[a]

	config	ΔE_{ads}	$O_{w1}-H_{w1}$	$O_{w1}-H_{w2}$	$O_{br1}-H_{w1}$	$O_{br2}-H_{w2}$	M_1-O_{w1}	M_1-O_{w2}
				(110)				
TiO_2	*4mol*	−99.9	1.005	2.132	1.737	1.738	2.309	2.309
	2mol/2diss	−85.8	1.574	1.733	1.042	1.880	2.045	2.232
RuO_2	*4mol*	−138.0	0.981	2.281	1.728	1.889	2.231	2.253
	2mol/2diss	−147.7	1.524	1.689	0.995	2.117	2.131	2.215
IrO_2	*4diss*	−210.5	1.759	2.350	1.019	1.019	2.002	2.000
				(011)				
TiO_2	*8mol*	−126.7	1.025	1.898	1.561	1.561	2.242	2.231
	4mol/4diss	−123.7	1.557	1.736	1.026	1.664	1.970	2.257
RuO_2	*6mol/2diss*	−130.4	1.510	1.514	1.035	2.705	2.067	2.173
	4mol/4diss	−130.8	1.591	1.531	1.024	2.049	2.099	2.175
IrO_2	*4mol/4diss*	−156.7	1.598	1.503	1.021	2.410	2.030	2.141
	3mol/5diss	−160.7	1.512	1.499	1.042	2.505	2.057	2.135
	2mol/6diss	−172.8	1.458	1.679	1.069	1.534	2.060	2.102

[a]See Figure 5 for water labels.

preferred one on RuO_2 and IrO_2. This can be related to the different behavior observed regarding the water adsorption energies on (110) and (011). The interaction energy of water on TiO_2 (110) is smaller than on TiO_2 (011), whereas for RuO_2 and IrO_2 the reverse trend is observed. Such differences arise from the nature of the vacant site (axial or equatorial) on each surface and on the octahedral distortion observed in the bulk of each material: tetragonal elongation for TiO_2 (axial bonds are larger than equatorial ones) and tetragonal compression for RuO_2 and IrO_2 (axial bonds are shorter than equatorial ones). As mentioned above, the vacant site of M_{5c} in the (110) surface is axial, whereas the vacant site of M_{5c} in the (011) surface is equatorial. Thus, for TiO_2, interaction of water with the axial vacant site of M_{5c} in (110)-TiO_2 is smaller than the interaction with the equatorial vacant site of (011)-TiO_2, whereas the opposite is observed for RuO_2 and IrO_2. The larger the interaction is, the larger the increase of acidity of the water molecule, which would explain that the proton transfer to O_{br} occurs more easily on (011) than on (110) for TiO_2 and on (110) than on (011) for RuO_2 and IrO_2. Among these latter materials, relative energies indicate that deprotonation on (011), although unfavorable in both cases, is less difficult on IrO_2 (7.0 kJ mol^{-1}) than on RuO_2 (12.6 kJ mol^{-1}) as found for (110).

Differences in structural parameters and net atomic charges are consistent with this explanation. For TiO_2, $M-O_w$ and $O_{br}-H_w$ distances are larger on the (110) surface (2.251 and 1.794 Å) than on the (011) one (2.103 and 1.510 Å). In line with these findings, the net charge of the water molecule when adsorbed in (110)-TiO_2 is 0.069 a.u and 0.075 in (011)-TiO_2. In contrast, for RuO_2, the values of these distances follow the opposite trend; that is, $M-O_w$ and $O_{br}-H_w$ distances on the (110)-RuO_2 surface (2.172 and 1.588 Å) are shorter than on the (011)-RuO_2 one (2.177 and 1.615 Å) and the net charge of water is 0.104 when adsorbed on (110)-RuO_2 and 0.076 on (110)-RuO_2. For IrO_2, we could not locate the *mol* form on the (110) surface. The trends observed on the electron transfer from water to the metal oxides are in agreement with the fact that metal d-bands above the Fermi level are higher for TiO_2 than for RuO_2 and IrO_2 (see Figure 4), which would explain the smaller electron donation from water to the metal and weaker bond in the former case.

Overall, the ability of (110) and (011) surfaces to induce dissociation of an interacting water molecule seems to be ultimately related to (i) the kind of octahedral distortion observed in the bulk of these materials (tetragonal elongation for TiO_2 and tetragonal compression for RuO_2 and IrO_2) and (ii) the different nature of the vacant sites created (axial or equatorial) on these surfaces.

Adsorption of Water Monolayer. Previous section has shown that the relative stability between the *mol* and *diss* adsorbed forms of water on the (110) and (011) surfaces of MO_2 (M = Ti, Ru, and Ir) depends on the increase of water acidity upon adsorption and on the basicity of O_{br}. These factors depend on the metal oxide and on the different nature of the M_{5c} vacant at each surface. At higher water coverages, however, cooperative H-bond interactions can come into play in determining whether deprotonation occurs or not. Thus, we have analyzed the structure of a water monolayer on each surface and metal oxide. For that, we have added one water molecule at each of the unsaturated metal centers; that is, four molecules per unit cell at the (110) surface and eight water molecules at the (011) one. We considered all possible combinations of *mol* and *diss* water molecules as initial structures. For instance, for the (110) surface, we considered seven possible structures: (i) 4 undissociated (molecular) water molecules (*4mol*), (ii) 3 molecular and 1 dissociated (*3mol/1diss*), (iii) *2mol/2diss*, (iv) *1mol/3diss*, and (v) *4diss*. Note that for the *2mol/2diss* configuration three different starting situations are possible, two in which the two equal molecules (*mol* or *diss*) are neighbors and another one in which they are not. All possible combinations were also considered for the (011) surface. Adsorption energies per water molecule and structural parameters of main configurations are given in Table 4. Figure 5 shows the optimized structures of the most stable configuration of each material and surface.

First of all, it can be observed that the adsorption energy per water molecule in the monolayer is in all cases except (110)-IrO_2 and (011)-TiO_2 larger (in absolute value) than that of a single water molecule, which indicates the presence of cooperative effects as a result of the formation of H-bond chains of moderate strength. Indeed, Figure 5 shows that two parallel H-bond chains separated by O_{br} are formed for both the (110) and (011) surfaces. Increases on the adsorption energy per water molecule range from 10 to 30 kJ mol^{-1} and result from a subtle balance between the changes induced on the water−surface interaction, which decreases as indicated by

DOI: 10.1021/acsomega.8b03350
ACS Omega 2019, 4, 2989−2999

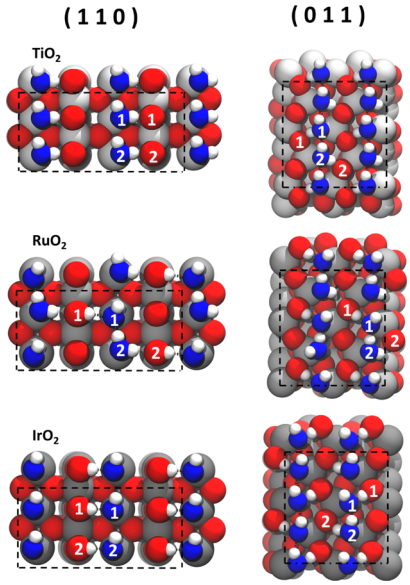

Figure 5. Most stable configuration at the PBE-D2 level of theory for the water monolayer interacting with MO_2 (M = Ti, Ru, and Ir). The numbers 1 and 2 refer to interacting water molecules and define the main structural parameters included in Table 4.

the increase of the M−O distance, and the stabilizing H-bond interactions between the water molecules in the monolayer. At the (110)-IrO_2 surface, the adsorption energy per water molecule is essentially the same than that obtained for the isolated water molecule because the H-bonding at this surface is the weakest one; that is, the O_{w1}−H_{w2} distance (2.350 Å) is the largest one. At the (011)-TiO_2 surface, the adsorption energy is smaller in the monolayer because there is a significant increase of the M−O distance (see Tables 3 and 4).

Most stable monolayer configuration depends on the material and on the surface. For (110)-TiO_2, the most stable arrangement is that in which no water molecules are dissociated (4*mol*), whereas for (110)-RuO_2, the preferred configuration has a 50% degree of deprotonation (2*mol*/2*diss*) and for (110)-IrO_2, the only configuration located exhibits a 100% degree of deprotonation (4*diss*). This trend is in agreement with what was found for the adsorption of a single water molecule, which showed that the preference for dissociation increases from TiO_2 to RuO_2 and to IrO_2. Indeed, for the latter material only the dissociated form was localized (see Table 3). For RuO_2, the 2*mol*/2*diss* situation is more stable than the 4*diss*, despite the dissociation of a single water molecule being the preferred situation (Table 3), because it allows forming very stable $H_3O_2^-$ species. That is, this 2*mol*/2*diss* configuration encloses two $H_3O_2^-$ species resulting from deprotonation of two water molecules to two O_{br}. This deprotonation leads to OH^- species that, due to their higher basicity, establish strong hydrogen bonds (∼1.7 Å) with the undissociated water molecules. Furthermore, as already seen previously for H_2O−RuO_2,[21] the M−OH interaction involves a significant electron donation to the surface that accumulates on the O_{br} so that the charge of the $H_3O_2^-$ species is smaller than 1. For IrO_2, the water−surface interaction dominates, in agreement with its much larger interaction energy (see Table 3) and higher surface energy (Table 2) and all water molecules dissociate. In this situation, H-bonding between metal-coordinated OH− is very weak, and thus, adsorption energy per water molecule is essentially the same as that of an isolated molecule.

For the (011) surface, we observe similar trends; that is, the most stable arrangement (011)-TiO_2 is that in which no water molecules are dissociated (8*mol*), whereas for (011)-RuO_2 and (011)-IrO_2, the preferred configurations exhibit a 50% (4*mol*/4*diss*) and 75% (2*mol*/6*diss*) degree of deprotonation, respectively. In this case, the observed trends are not in agreement with that found for the adsorption of a single water molecule, which shows that the dissociated form is the preferred situation for TiO_2 and the molecular form the preferred one for RuO_2 and IrO_2. This is due to the fact that the presence of the monolayer modifies the water−surface interaction as compared to that with a single molecule. For TiO_2, the adsorption energy per water molecule in the monolayer is smaller than in the single water adsorption. Indeed, the Ti−O distance is significantly larger in the former (2.24 vs 2.10 Å). Such an increase in the M−O distance is produced to establish an efficient H-bond network but weakens the water−surface interaction, leading to a smaller increase of water acidity that hinders deprotonation. Still, the configuration with 50% dissociation, that is, with two $H_3O_2^-$ and two protonated O_{br}, is only 3 kJ mol^{-1} less stable than the fully undissociated one (Table 4), and thus, the present results are not conclusive about whether water monolayer at the (110)-TiO_2 surface is dissociated or not. Furthermore, thermal effects need to be taken into account.

For (011)-RuO_2, the most stable configuration encloses four molecular and four dissociated waters; that is, it shows a 50% degree of deprotonation, as in the (110) surface. Note that we have not been able to localize a minimum corresponding to the fully undissociated monolayer. Attempts to optimize such a structure collapsed to (6*mol*/2*diss*), the second most representative structure. This behavior is in contrast with the fact that isolated water prefers a molecular adsorbed form. However, formation of $H_3O_2^-$ species, with a strong H-bond between the OH^- and the undissociated water molecule, is particularly favorable. A 50% deprotonation is the preferred situation as it maximizes the number of $H_3O_2^-$ units and hence H-bond cooperative effects.

For (011)-IrO_2, the preferred configuration shows a 75% deprotonation (2*mol*/6*diss*), despite the molecular form being the most stable for the isolated water molecule, although with a lower relative energy as compared to RuO_2. This 75% deprotonation does not maximize the number of $H_3O_2^-$, as one would expect, because water surface interaction dominates over H-bonding. Furthermore, as already seen for RuO_2,[21] adsorption cooperative effects may induce deprotonation. That is, deprotonation of one water molecule favors deprotonation of a neighbor adsorbed water because of the increase of the metal Lewis acidity as a result of the protonation of O_{br}. Overall, the degree of deprotonation results from a subtle balance between H-bond cooperativity and adsorption cooperativity. In the case of IrO_2, the latter effect is larger because of the larger interaction with the metal sites.

Present results show that relative energies corresponding to lower *mol*/*diss* configuration arrangements per water molecule are small (3−16 kJ mol^{-1}) and thus may contribute to the behavior of the water−metal oxide interface. On the other hand, thermal effects may modify the relative stability of these configurations. Because of that, we have run AIMDs up to 8 ps (1 ps equilibration) for all metal oxides and the two surfaces starting from the most stable monolayer obtained with static

DOI: 10.1021/acsomega.8b03350
ACS Omega 2019, 4, 2989−2999

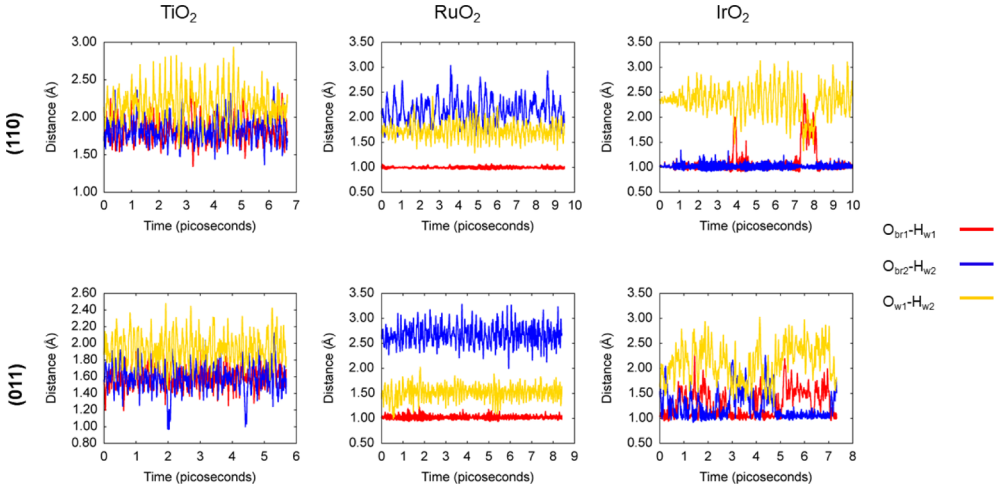

Figure 6. H-bond distances of two neighbor water molecules (in Å) along the dynamics. See Figure 5 for labeling.

calculations. Figure 6 shows the H-bond distances corresponding to two interacting water molecules and those between these water molecules and O_{br} along the simulation. M−O distances are reported in Figure S1 of the Supporting Information. Table 5 shows the frequency of each possible configuration, considering that proton transfer to an O_{br} occurs if the H-bond distance is smaller than 1.2 Å.

Table 5. Percentage of Configurations with Different Degree of Water Deprotonation on the (110) and (011) Surfaces of MO_2 (M = Ti, Ru, and Ir)

	TiO_2	RuO_2	IrO_2
	(110)		
4mol	100.0	0.0	0.0
3mol/1diss	0.0	0.0	0.0
2mol/2diss	0.0	99.9	4.8
1mol/3diss	0.0	0.1	11.4
4diss	0.0	0.00	83.7
	(011)		
8mol	94.3	0.0	0.0
7mol/1diss	5.7	0.0	0.0
6mol/2diss	0.0	1.11	0.0
5mol/3diss	0.0	22.7	2.6
4mol/4diss	0.0	71.8	33.5
3mol/5diss	0.0	4.4	42.7
2mol/6diss	0.0	0.0	19.5
1mol/7diss	0.0	0.0	1.4
8diss	0.0	0.0	0.3

For (110)-TiO_2 and (110)-RuO_2, the most stable configurations (*4mol* and *2mol/2diss*, respectively) remain along the 7−8 ps simulation. For (110)-TiO_2, the O_{br}−H_w H-bond distance oscillates around 1.7 Å, whereas the H-bond distance between the two water molecules oscillates around 2.1 Å. In the latter case, oscillations are larger because of the weaker H-bond. For (110)-RuO_2, H-bond distances are consistent with the presence of $H_3O_2^-$ species and a protonated O_{br} almost all along the simulation. Note that the frequency of the *2mol/2diss* is 99.9% and only the *1mol/3diss* arrangement appears in 0.1%. For IrO_2, we observed a larger proton mobility. As predicted by static calculations, the main configuration is a fully dissociated monolayer (*4diss*) with an 84% frequency. Noticeably, there is a non-negligible frequency of the *1mol/3diss* (11.4%) and of the *2mol/2diss* (4.8%). This indicates that thermal effects disfavor deprotonation, because of the increase of the M−O_w distances, which reduces the water−surface interaction and thus the water acidity.

The (011) surface shows a larger proton mobility compared to the (110) one. For TiO_2 and RuO_2, most stable configurations (*8mol* and *4mol/4diss*, respectively) obtained from static calculations remain the most frequent arrangement (94 and 72%). However, for IrO_2, the most stable configuration (*2mol/6diss*) is no longer the main one when including thermal effects. Indeed, three configurations account for a frequency of 95%: *4mol/4diss* with 33%, *3mol/5diss* with 43%, and *2mol/6diss* with 19%. Note that the most frequent configuration (*3mol/5diss*) does not correspond to the most stable one obtained from static calculations (*2mol/6diss*). These results again show that thermal effects tend to decrease the M−OH_2 interactions, thereby increasing the percentage of molecular water.

CONCLUSIONS

The present study analyzes the H_2O−MO_2 (M = Ti, Ru, and Ir) interactions by means of periodic DFT (PBE-D2) calculations. Adsorption of both an isolated water molecule and a full monolayer on the two surfaces that mostly contribute to the Wulff shape, the (110) and (011) surfaces, has been addressed. Results indicate that the adsorption of a single molecule preferably occurs in its molecular form on the (110)-TiO_2 surface and in its dissociative form on (110)-RuO_2 and (110)-IrO_2. However, the opposite trend is observed on the (011) surface; that is, water prefers to adsorb in its dissociative form on (011)-TiO_2 and in its molecular form on (011)-RuO_2 and (011)-IrO_2. This is related to the kind of octahedral distortion observed in the bulk of these materials (tetragonal elongation for TiO_2 and tetragonal compression for RuO_2 and IrO_2) and to the different nature of the vacant sites created on these surfaces, axial on (110) and equatorial on (011). Thus, water adsorption on TiO_2 leads to longer M−O distances on (110) than on (011), and consequently, the increase of water acidity (and possible dissociation) is larger on (011). The opposite is observed for RuO_2 and IrO_2 with longer M−O distances on (011). Furthermore, adsorption energies (in absolute value) increase from TiO_2 to RuO_2 and IrO_2, along with the electron transfer from the water molecule to MO_2.

DOI: 10.1021/acsomega.8b03350
ACS Omega 2019, 4, 2989−2999

For the monolayer, in addition to the intrinsic water adsorption, other effects such as cooperative H-bond interactions, particularly the formation of $H_3O_2^-$ species, and cooperative adsorption come into play in determining whether deprotonation occurs or not. Furthermore, thermal effects seem to favor configurations with a smaller degree of dissociation because of an enlargement of M−O distances, which leads to a smaller increase of water acidity. For TiO_2, water monolayer is fully undissociated on both (110) and (011) surfaces, whereas for RuO_2, water monolayer exhibits a 50% dissociation, the formation of $H_3O_2^-$ motifs being essential. Finally, on (110)-IrO_2, the main monolayer configuration is the fully dissociated one, whereas on (011)-IrO_2, it exhibits a degree of dissociation that ranges from 50 to 75%. Overall, the present study shows that several effects, in addition to the intrinsic water adsorption, are responsible for the degree of dissociation of adsorbed water on MO_2 (M = Ti, Ru, and Ir), IrO_2 being the one more prone to induce dissociation.

COMPUTATIONAL DETAILS

Periodic boundary DFT calculations were carried out with the Vienna ab initio simulation package (VASP) code.[54,55] All calculations were performed with the GGA PBE functional[56] plus D2 Grimme's correction[57] for dispersion and using the projector augmented wave pseudopotentials[58,59] to describe ionic cores and valence electrons through a plane wave basis with a kinetic energy cutoff equal to 500 eV. The above computational parameters ensure a good agreement with experimental cell parameters of the bulk structures for all the studied materials (TiO_2, RuO_2, IrO_2). Moreover, the inclusion of dispersion corrections is essential to describe properly adsorption processes[60] and bulk water.[61,62] Bulk calculations were performed considering a *K*-point mesh for the Brillouin zone of (8,8,8), (15,15,15), and (9,9,9) for TiO_2, RuO_2, and IrO_2, respectively, employing the Monkhorst−Pack (MP) grid,[63] whereas slab calculations were performed considering a MP *K*-point mesh of (3,3,1), (6,6,1), and (4,4,1) for TiO_2, RuO_2, and IrO_2, respectively. The cutoff and *K*-point mesh were chosen according to the best cost/accuracy strategy of both cell parameters and surface energies. The energy convergence criteria for electronic and geometry relaxations were fixed to 10^{-5} and 10^{-4} eV, respectively.

Because the water adsorption mode on TiO_2 has been controversial and sensitive to the computational approach,[7,10] we have performed additional calculations for this system with a hybrid functional PBE0[64] and considering the D3 correction for dispersion[65] (see Table S1 of the Supporting Information). Results obtained at the PBE0-D2 and PBE-D3 levels of theory show that although adsorption energies can vary up to 13 kJ mol^{-1} with respect to PBE-D2, relative energies between the molecular and dissociative forms follow the same trend and vary less than 3.5 kJ mol^{-1}, which shows the robustness of the chosen approximation.

Surface models of the main crystallographic orientations were built by cutting out the slab from the optimized bulk structure. Slabs were constructed considering a (2 × 1) supercell and a four-layer thickness, the minimum one for a reasonable converged surface energy (see Figure S2 of the Supporting Information). The c value was set to 35 Å ensuring an interlayer distance of at least 21 Å to minimize the interaction between replicas in the (*h k l*) perpendicular direction. Atom positions were fully relaxed in the optimization process. Surface energies of the (110) and (011) facets were computed through the following equation:

$$\gamma_{(hkl)} = \frac{E_{slab} - (N \cdot E_{bulk})}{2 \cdot A} \quad (1)$$

where E_{slab} is the energy corresponding to the relaxed surface without optimizing the bulk cell parameters; E_{bulk} is the fully relaxed bulk energy; N is the number of formula units in the slab per units in the bulk unit cell; and $2A$ is the corresponding two cross-sectional area of the slab.

Water adsorption on the two most stable facets of the rutile polymorph, that is, (110) and (011), was simulated with a (2 × 2) supercell in both the low and high coverage regimes. The low coverage regime corresponds to the adsorption of only one water molecule per unit cell, whereas in the high coverage regime, all the outermost (undercoordinated) metal atoms were saturated with water molecules, leading to a water monolayer. Reported adsorption energies are normalized per water molecule, according to the following equation:

$$\Delta E_{ads} = \frac{E_{(hkl)+H_2O} - E_{(hkl)} - (n_{H_2O} \cdot E_{H_2O})}{n_{H_2O}} \quad (2)$$

where $E_{(hkl)+H_2O}$ is the total energy of the slab with the adsorbed water, $E_{(hkl)}$ is the total energy of the slab model, E_{H_2O} is the total energy of an isolated water inside a 15 × 15 × 15 $Å^3$ cubic box, and $n_{(H_2O)}$ is the number of adsorbed waters onto the surfaces. The properties of these materials and their propensity to induce water deprotonation are discussed in terms of pDOS and Bader charge analysis.[66−68]

At this point, it is worth mentioning that TiO_2 is particularly sensitive to the computational model used.[7] Concerning the slab thickness of the (110) surface, our calculations show, as found previously,[36] an even odd oscillation on the water adsorption energy with the number of TiO_2 layers (see Table S2 of the Supporting Information). Most accurate results, given by a six- or seven-layer TiO_2 slab, provide the molecular form as the more stable one, as found experimentally.[9] Because of computational reasons, and for consistency with RuO_2 and IrO_2, present calculations correspond to a four-layer TiO_2 slab. This model provides the correct relative stability between the molecular and dissociative forms, although with a relative energy (34.7 kJ mol^{-1}) that is significantly higher than that recently determined by combining supersonic molecular beam, STM, and AIMD (3.5 kJ mol^{-1}).[9] Regarding the (011) surface, it is worth mentioning that depending on the number of layers, the surface may present a significant reconstruction, as observed experimentally.[11] This involves the cleavage of two internal Ti−O bonds to strengthen the Ti−O bonds with the surface undercoordinated Ti_{5c} sites (see Figure S3 of the Supporting Information). The energy difference between the non-reconstructed and the reconstructed one is small (Figure S4), and the former surface has a higher surface energy.

AIMDs were carried out on the most stable water monolayer structures (i.e., the one with the most stable deprotonation degree) for both (110) and (011) surfaces for all the materials. The energy convergence criteria were fixed to 10^{-4} eV. AIMDs were carried out considering an equilibration period of 1 ps (1000 steps of 1 ft) and a production period of 7 ps (7000 steps of 1 ft) in the *NVT* ensemble. During both the equilibration and the production periods, only the water monolayer and the first layer of the surface were allowed to

DOI: 10.1021/acsomega.8b03350
ACS Omega 2019, 4, 2989−2999

move according to the motion's equations, while atoms of the remaining surface layers were maintained at fixed positions. This option was chosen in order to avoid unrealistic deformation of the structure of the slabs and to simulate the actual rigidity of the material.

■ ASSOCIATED CONTENT

Supporting Information

The Supporting Information is available free of charge on the ACS Publications website at DOI: 10.1021/acsomega.8b03350.

PBE-D2 surface energies with different slab thicknesses; optimized structures for the TiO_2 (011) rutile surface; M−O distances along the AIMD; and relative energies between molecular and dissociative adsorbed forms on the TiO_2 (110) rutile surface, as a function of the number of layers (PDF)

■ AUTHOR INFORMATION

Corresponding Authors

*E-mail: xavier.solans@uab.cat (X.S.-M.).
*E-mail: mariona.sodupe@uab.cat (M.S.).

ORCID

Javier Heras-Domingo: 0000-0002-4322-3146
Stefano Pantaleone: 0000-0002-2457-1065
Albert Rimola: 0000-0002-9637-4554
Luis Rodríguez-Santiago: 0000-0003-4983-4228
Mariona Sodupe: 0000-0003-0276-0524

Author Contributions

†D.G., J.H.-D., and S.P. have equally contributed.

Notes

The authors declare no competing financial interest.

■ ACKNOWLEDGMENTS

The authors gratefully acknowledge financial support from MINECO (CTQ2017-89132-P) and the Generalitat de Catalunya (2017SGR-1323). X.S.-M. is grateful for the Professor Agregat Serra Hunter position. A.R. is indebted to "Ramon y Cajal" program.

■ REFERENCES

(1) Suen, N.-T.; Hung, S.-F.; Quan, Q.; Zhang, N.; Xu, Y.-J.; Chen, H. M. Electrocatalysis for the Oxygen Evolution Reaction: Recent Development and Future Perspectives. *Chem. Soc. Rev.* **2017**, *46*, 337−365.

(2) Paoli, E. A.; Masini, F.; Frydendal, R.; Deiana, D.; Schlaup, C.; Malizia, M.; Hansen, T. W.; Horch, S.; Stephens, I. E. L.; Chorkendorff, I. Oxygen evolution on well-characterized mass-selected Ru and RuO_2 nanoparticles. *Chem. Sci.* **2015**, *6*, 190−196.

(3) Reier, T.; Oezaslan, M.; Strasser, P. Electrocatalytic Oxygen Evolution Reaction (OER) on Ru, Ir, and Pt Catalysts: A Comparative Study of Nanoparticles and Bulk Materials. *ACS Catal.* **2012**, *2*, 1765−1772.

(4) Walter, M. G.; Warren, E. L.; McKone, J. R.; Boettcher, S. W.; Mi, Q.; Santori, E. A.; Lewis, N. S. Solar Water Splitting Cells. *Chem. Rev.* **2010**, *110*, 6446−6473.

(5) Song, F.; Bai, L.; Moysiadou, A.; Lee, S.; Hu, C.; Liardet, L.; Hu, X. Transition Metal Oxides as Electrocatalysts for the Oxygen Evolution Reaction in Alkaline Solutions: An Application-Inspired Renaissance. *J. Am. Chem. Soc.* **2018**, *140*, 7748−7759.

(6) Yin, W.-J.; Wen, B.; Zhou, C.; Selloni, A.; Liu, L.-M. Excess electrons in reduced rutile and anatase TiO_2. *Surf. Sci. Rep.* **2018**, *73*, 58−82.

(7) Diebold, U. Perspective: A Controversial Benchmark System for Water-Oxide Interfaces: $H_2O/TiO_2(110)$. *J. Chem. Phys.* **2017**, *147*, 040901.

(8) Serrano, G.; Bonanni, B.; Di Giovannantonio, M.; Kosmala, T.; Schmid, M.; Diebold, U.; Di Carlo, A.; Cheng, J.; VandeVondele, J.; Wandelt, K.; Goletti, C. Molecular Ordering at the Interface Between Liquid Water and Rutile $TiO_2(110)$. *Adv. Mater. Interfaces* **2015**, *2*, 1500246.

(9) Wang, Z.-T.; Wang, Y.-G.; Mu, R.; Yoon, Y.; Dahal, A.; Schenter, G. K.; Glezakou, V.-A.; Rousseau, R.; Lyubinetsky, I.; Dohnálek, Z. Probing equilibrium of molecular and deprotonated water on $TiO_2(110)$. *Proc. Natl. Acad. Sci. U.S.A.* **2017**, *114*, 1801−1805.

(10) Sun, C.; Liu, L.-M.; Selloni, A.; Lu, G. Q.; Smith, S. C.; Smith, S. C. Titania-Water Interactions: A Review of Theoretical Studies. *J. Mater. Chem.* **2010**, *20*, 10319.

(11) Balajka, J.; Aschauer, U.; Mertens, S. F. L.; Selloni, A.; Schmid, M.; Diebold, U. Surface Structure of TiO_2 Rutile (011) Exposed to Liquid Water. *J. Phys. Chem. C* **2017**, *121*, 26424−26431.

(12) Mu, R.; Zhao, Z.-j.; Dohnálek, Z.; Gong, J. Structural Motifs of Water on Metal Oxide Surfaces. *Chem. Soc. Rev.* **2017**, *46*, 1785−1806.

(13) Siahrostami, S.; Vojvodic, A. Influence of Adsorbed Water on the Oxygen Evolution Reaction on Oxides. *J. Phys. Chem. C* **2014**, *119*, 1032−1037.

(14) Zhang, Z.; Bondarchuk, O.; Kay, B. D.; White, J. M.; Dohnálek, Z. Imaging Water Dissociation on $TiO_2(110)$: Evidence for Inequivalent Geminate OH Groups. *J. Phys. Chem. B* **2006**, *110*, 21840−21845.

(15) Bikondoa, O.; Pang, C. L.; Ithnin, R.; Muryn, C. A.; Onishi, H.; Thornton, G. Direct visualization of defect-mediated dissociation of water on $TiO_2(110)$. *Nat. Mater.* **2006**, *5*, 189−192.

(16) Ketteler, G.; Yamamoto, S.; Bluhm, H.; Andersson, K.; Starr, D. E.; Ogletree, D. F.; Ogasawara, H.; Nilsson, A.; Salmeron, M. The Nature of Water Nucleation Sites on $TiO_2(110)$ Surfaces Revealed by Ambient Pressure X-Ray Photoelectron Spectroscopy. *J. Phys. Chem. C* **2007**, *111*, 8278−8282.

(17) Björneholm, O.; Hansen, M. H.; Hodgson, A.; Liu, L.-M.; Limmer, D. T.; Michaelides, A.; Pedevilla, P.; Rossmeisl, J.; Shen, H.; Tocci, G.; Tyrode, E.; Walz, M.-M.; Werner, J.; Bluhm, H. Water at Interfaces. *Chem. Rev.* **2016**, *116*, 7698−7726.

(18) Mu, R.; Cantu, D. C.; Glezakou, V.-A.; Lyubinetsky, I.; Rousseau, R.; Dohnálek, Z. Deprotonated Water Dimers: The Building Blocks of Segmented Water Chains on Rutile $RuO_2(110)$. *J. Phys. Chem. C* **2015**, *119*, 23552−23558.

(19) Mu, R.; Cantu, D. C.; Lin, X.; Glezakou, V.-A.; Wang, Z.; Lyubinetsky, I.; Rousseau, R.; Dohnálek, Z. Dimerization Induced Deprotonation of Water on $RuO_2(110)$. *J. Phys. Chem. Lett.* **2014**, *5*, 3445−3450.

(20) Nguyen, M.-T.; Mu, R.; Cantu, D. C.; Lyubinetsky, I.; Glezakou, V.-A.; Dohnálek, Z.; Rousseau, R. Dynamics, Stability, and Adsorption States of Water on Oxidized $RuO_2(110)$. *J. Phys. Chem. C* **2017**, *121*, 18505−18515.

(21) Rao, R. R.; Kolb, M. J.; Hwang, J.; Pedersen, A. F.; Mehta, A.; You, H.; Stoerzinger, K. A.; Feng, Z.; Zhou, H.; Bluhm, H.; Giordano, L.; Stephens, I. E. L.; Shao-Horn, Y. Surface Orientation Dependent Water Dissociation on Rutile Ruthenium Dioxide. *J. Phys. Chem. C* **2018**, *122*, 17802−17811.

(22) Heras-Domingo, J.; Sodupe, M.; Solans-Monfort, X. Interaction between Ruthenium Oxide Surfaces and Water Molecules. Effect of Surface Morphology and Water Coverage. *J. Phys. Chem. C* **2018**, DOI: 10.1021/acs.jpcc.8b06438.

(23) Lobo, A.; Conrad, H. Interaction of H_2O with the $RuO_2(110)$ Surface Studied by HREELS and TDS. *Surf. Sci.* **2003**, *523*, 279−286.

(24) Jaimes, R.; Vazquez-Arenas, J.; González, I.; Galván, M. Theoretical evidence of the relationship established between the HO radicals and H_2O adsorptions and the electroactivity of typical catalysts used to oxidize organic compounds. *Electrochim. Acta* **2017**, *229*, 345−351.

DOI: 10.1021/acsomega.8b03350
ACS Omega 2019, 4, 2989−2999

(25) Kuo, D.-Y.; Kawasaki, J. K.; Nelson, J. N.; Kloppenburg, J.; Hautier, G.; Shen, K. M.; Schlom, D. G.; Suntivich, J. Influence of Surface Adsorption on the Oxygen Evolution Reaction on IrO_2(110). *J. Am. Chem. Soc.* **2017**, *139*, 3473−3479.
(26) Sasahara, A.; Tomitori, M. An Atomic-Scale Study of TiO_2(110) Surfaces Exposed to Humid Environments. *J. Phys. Chem. C* **2016**, *120*, 21427−21435.
(27) Brookes, I. M.; Muryn, C. A.; Thornton, G. Imaging Water Dissociation on TiO_2(110). *Phys. Rev. Lett.* **2001**, *87*, 266103.
(28) Matthiesen, J.; Hansen, J. Ø.; Wendt, S.; Lira, E.; Schaub, R.; Lægsgaard, E.; Besenbacher, F.; Hammer, B. Formation and Diffusion of Water Dimers on Rutile TiO_2(110). *Phys. Rev. Lett.* **2009**, *102*, 226101.
(29) Lee, J.; Sorescu, D. C.; Deng, X.; Jordan, K. D. Water Chain Formation on TiO_2(110). *J. Phys. Chem. Lett.* **2012**, *4*, 53−57.
(30) Kimmel, G. A.; Baer, M.; Petrik, N. G.; VandeVondele, J.; Rousseau, R.; Mundy, C. J. Polarization- and Azimuth-Resolved Infrared Spectroscopy of Water on TiO_2(110): Anisotropy and the Hydrogen-Bonding Network. *J. Phys. Chem. Lett.* **2012**, *3*, 778−784.
(31) Henderson, M. A. An HREELS and TPD Study of Water on TiO_2(110): The Extent of Molecular versus Dissociative Adsorption. *Surf. Sci.* **1996**, *355*, 151−166.
(32) Walle, L. E.; Borg, A.; Uvdal, P.; Sandell, A. Experimental Evidence for Mixed Dissociative and Molecular Adsorption of Water on a Rutile TiO_2(110). *Phys. Rev. B: Condens. Matter Mater. Phys.* **2009**, *80*, 235436.
(33) Duncan, D. A.; Allegretti, F.; Woodruff, D. P. Water Does Partially Dissociate on the Perfect TiO_2 (110) Surface: A Quantitative Structure Determination. *Phys. Rev. B: Condens. Matter Mater. Phys.* **2012**, *86*, 045411.
(34) Diebold, U. The Surface Science of Titanium Dioxide. *Surf. Sci. Rep.* **2003**, *48*, 53−229.
(35) Gutiérrez Moreno, J. J.; Fronzi, M.; Lovera, P.; O'Riordan, A.; Nolan, M. Stability of Adsorbed Water on TiO2-TiN Interfaces. A First-Principles and Ab Initio Thermodynamics Investigation. *J. Phys. Chem. C* **2018**, *122*, 15395−15408.
(36) Kowalski, P. M.; Meyer, B.; Marx, D. Composition, Structure, and Stability of the Rutile TiO_2. *Phys. Rev. B: Condens. Matter Mater. Phys.* **2009**, *79*, 115410.
(37) Kumar, N.; Kent, P. R. C.; Wesolowski, D. J.; Kubicki, J. D. Modeling Water Adsorption on Rutile (110) Using van Der Waals Density Functional and DFT+U Methods. *J. Phys. Chem. C* **2013**, *117*, 23638−23644.
(38) Nilsson, J. O.; Leetmaa, M.; Wang, B.; Žguns, P. A.; Pašti, I.; Sandell, A.; Skorodumova, N. V. Modeling Kinetics of Water Adsorption on the Rutile TiO_2 (110) Surface: Influence of Exchange-Correlation Functional. *Phys. Status Solidi B* **2017**, *255*, 1700344.
(39) Hosseinpour, S.; Tang, F.; Wang, F.; Livingstone, R. A.; Schlegel, S. J.; Ohto, T.; Bonn, M.; Nagata, Y.; Backus, E. H. G. Chemisorbed and Physisorbed Water at the TiO_2/Water Interface. *J. Phys. Chem. Lett.* **2017**, *8*, 2195−2199.
(40) Calegari Andrade, M. F.; Ko, H.-Y.; Car, R.; Selloni, A. Structure, Polarization, and Sum Frequency Generation Spectrum of Interfacial Water on Anatase TiO_2. *J. Phys. Chem. Lett.* **2018**, *9*, 6716−6721.
(41) Liu, L.-M.; Zhang, C.; Thornton, G.; Michaelides, A. Structure and Dynamics of Liquid Water on Rutile TiO_2(110). *Phys. Rev. B: Condens. Matter Mater. Phys.* **2010**, *82*, 161415.
(42) Agosta, L.; Brandt, E. G.; Lyubartsev, A. P. Diffusion and Reaction Pathways of Water near Fully Hydrated TiO_2 Surfaces from Ab Initio Molecular Dynamics. *J. Chem. Phys.* **2017**, *147*, 024704.
(43) Torrelles, X.; Cabailh, G.; Lindsay, R.; Bikondoa, O.; Roy, J.; Zegenhagen, J.; Teobaldi, G.; Hofer, W. A.; Thornton, G. Geometric Structure of TiO_2(011)(2×1). *Phys. Rev. Lett.* **2008**, *101*, 185501.
(44) Gong, X.-Q.; Khorshidi, N.; Stierle, A.; Vonk, V.; Ellinger, C.; Dosch, H.; Cheng, H.; Selloni, A.; He, Y.; Dulub, O.; Diebold, U. The 2×1 reconstruction of the rutile TiO_2(011) surface: A combined density functional theory, X-ray diffraction, and scanning tunneling microscopy study. *Surf. Sci.* **2009**, *603*, 138−144.
(45) Aschauer, U.; Selloni, A. Structure of the Rutile TiO_2(011) Surface in an Aqueous Environment. *Phys. Rev. Lett.* **2011**, *106*, 166102.
(46) Barnard, A. S.; Zapol, P.; Curtiss, L. A. Modeling the Morphology and Phase Stability of TiO_2 Nanocrystals in Water. *J. Chem. Theory Comput.* **2005**, *1*, 107−116.
(47) Di Valentin, C.; Tilocca, A.; Selloni, A.; Beck, T. J.; Klust, A.; Batzill, M.; Losovyj, Y.; Diebold, U. Adsorption of Water on Reconstructed Rutile TiO_2(011)-(2×1): TiO Double Bonds and Surface Reactivity. *J. Am. Chem. Soc.* **2005**, *127*, 9895−9903.
(48) Rao, R. R.; Kolb, M. J.; Halck, N. B.; Pedersen, A. F.; Mehta, A.; You, H.; Stoerzinger, K. A.; Feng, Z.; Hansen, H. A.; Zhou, H.; Giordano, L.; Rossmeisl, J.; Vegge, T.; Chorkendorff, I.; Stephens, I. E. L.; Shao-Horn, Y. Towards Identifying the Active Sites on RuO_2(110) in Catalyzing Oxygen Evolution. *Energy Environ. Sci.* **2017**, *10*, 2626−2637.
(49) Bolzan, A. A.; Fong, C.; Kennedy, B. J.; Howard, C. J. Structural Studies of Rutile-Type Metal Dioxides. *Acta Crystallogr., Sect. B: Struct. Sci.* **1997**, *53*, 373−380.
(50) Ping, Y.; Galli, G.; Goddard, W. A. Electronic Structure of IrO_2: The Role of the Metal d Orbitals. *J. Phys. Chem. C* **2015**, *119*, 11570−11577.
(51) Berlijn, T.; Snijders, P. C.; Delaire, O.; Zhou, H.-D.; Maier, T. A.; Cao, H.-B.; Chi, S.-X.; Matsuda, M.; Wang, Y.; Koehler, M. R.; Kent, P. R. C.; Weitering, H. H. Itinerant Antiferromagnetism in RuO_2. *Phys. Rev. Lett.* **2017**, *118*, 077201.
(52) Torun, E.; Fang, C. M.; de Wijs, G. A.; de Groot, R. A. Role of Magnetism in Catalysis: RuO_2 (110) Surface. *J. Phys. Chem. C* **2013**, *117*, 6353−6357.
(53) Novell-Leruth, G.; Carchini, G.; López, N. On the Properties of Binary Rutile MO_2 Compounds, M = Ir, Ru, Sn, and Ti: A DFT Study. *J. Chem. Phys.* **2013**, *138*, 194706.
(54) Kresse, G.; Furthmüller, J. Efficient iterative schemes forab initiototal-energy calculations using a plane-wave basis set. *Phys. Rev. B: Condens. Matter Mater. Phys.* **1996**, *54*, 11169−11186.
(55) Kresse, G.; Hafner, J. Ab initio molecular dynamics for liquid metals. *Phys. Rev. B: Condens. Matter Mater. Phys.* **1993**, *47*, 558−561.
(56) Perdew, J. P.; Burke, K.; Ernzerhof, M. Generalized Gradient Approximation Made Simple. *Phys. Rev. Lett.* **1996**, *77*, 3865−3868.
(57) Grimme, S. Accurate Description of van Der Waals Complexes by Density Functional Theory Including Empirical Corrections. *J. Comput. Chem.* **2004**, *25*, 1463−1473.
(58) Blöchl, P. E. Projector Augmented-Wave Method. *Phys. Rev. B: Condens. Matter Mater. Phys.* **1994**, *50*, 17953−17979.
(59) Kresse, G.; Joubert, D. From Ultrasoft Pseudopotentials to the Projector Augmented-Wave Method. *Phys. Rev. B: Condens. Matter Mater. Phys.* **1999**, *59*, 1758−1775.
(60) Rimola, A.; Costa, D.; Sodupe, M.; Lambert, J.-F.; Ugliengo, P. Silica Surface Features and Their Role in the Adsorption of Biomolecules: Computational Modeling and Experiments. *Chem. Rev.* **2013**, *113*, 4216−4313.
(61) Ohto, T.; Dodia, M.; Imoto, S.; Nagata, Y. Structure and Dynamics of Water at the Water-Air Interface Using First-Principles Molecular Dynamics Simulations within Generalized Gradient Approximation. *J. Chem. Theory Comput.* **2018**, *15*, 595−602.
(62) Gillan, M. J.; Alfè, D.; Michaelides, A. Perspective: How Good Is DFT for Water? *J. Chem. Phys.* **2016**, *144*, 130901.
(63) Monkhorst, H. J.; Pack, J. D. Special Points for Brillouin-Zone Integrations. *Phys. Rev. B: Solid State* **1976**, *13*, 5188−5192.
(64) Adamo, C.; Barone, V. Toward Reliable Density Functional Methods without Adjustable Parameters: The PBE0 Model. *J. Chem. Phys.* **1999**, *110*, 6158−6170.
(65) Grimme, S.; Antony, J.; Ehrlich, S.; Krieg, H. A Consistent and accurate ab initio parametrization of density functional dispersion correction (DFT-D) for the 94 elements H-Pu. *J. Chem. Phys.* **2010**, *132*, 154104.

DOI: 10.1021/acsomega.8b03350
ACS Omega 2019, 4, 2989−2999

(66) Bader, R. F. W. *Atoms in Molecules: A Quantum Theory*; Oxford University Press: New York, 1994.
(67) Yu, M.; Trinkle, D. R. Accurate and Efficient Algorithm for Bader Charge Integration. *J. Chem. Phys.* **2011**, *134*, 064111.
(68) Tang, W.; Sanville, E.; Henkelman, G. A Grid-Based Bader Analysis Algorithm without Lattice Bias. *J. Phys.: Condens. Matter* **2009**, *21*, 084204.

DOI: 10.1021/acsomega.8b03350
ACS Omega 2019, 4, 2989−2999